ChemComm

Chemical Communications

www.rsc.org/chemcomm

ROYAL SOCIETY
OF CHEMISTRY

COMMUNICATION
Kazuyoshi Kanamori *et al.*
Mechanically stable, hierarchically porous Cu$_3$(btc)$_2$ (HKUST-1) monoliths
via direct conversion of copper(II) hydroxide-based monoliths

Mechanically stable, hierarchically porous Cu₃(btc)₂ (HKUST-1) monoliths *via* direct conversion of copper(II) hydroxide-based monoliths†

Nirmalya Moitra,[a] Shotaro Fukumoto,[a] Julien Reboul,[b] Kenji Sumida,[b] Yang Zhu,[a] Kazuki Nakanishi,[a] Shuhei Furukawa,[b] Susumu Kitagawa[b] and Kazuyoshi Kanamori*[a]

The synthesis of highly crystalline macro-meso-microporous monolithic Cu₃(btc)₂ (HKUST-1; btc³⁻ = benzene-1,3,5-tricarboxylate) is demonstrated by direct conversion of Cu(OH)₂-based monoliths while preserving the characteristic macroporous structure. The high mechanical strength of the monoliths is promising for possible applications to continuous flow reactors.

Porous coordination polymers[1,2] (PCPs) or metal–organic frameworks (MOFs) assembled from metal ions with organic bridging units are of tremendous importance because of their possible applications in areas including gas storage, separation, catalysis, sensing, drug delivery, proton conduction, optics, biomedicine and microelectronics.[3] In order to maximize the performance of PCPs in such a diverse host of applications, it is necessary for fabrication techniques that deliver these materials in an appropriate material form to be developed. In recent years, there has been an increasing number of studies directed toward the structuralization of PCP crystallites into various material forms, such as hollow spheres,[4,5] core shell particles,[6] thin-films,[7] membranes,[8] patterns on surfaces,[9] coatings on monoliths,[10] and aerogels.[11] Many of these are achieved through synthetic strategies that result in the preferential deposition of PCPs at an appropriately functionalized surface,[12] and can be combined with techniques such as liquid-phase epitaxial growth,[13] seeding,[14] evaporation deposition[15] and electrochemistry for the preparation of high-quality PCP thin films, composites and crystal arrangements.[16] Despite the significant advances made in this regard, there is still a critical need for the development of fast and inexpensive methods that facilitate a greater control over material structuralization. In particular, porous materials that simultaneously offer a high effective surface area and efficient transport of fluids are crucial for the applications of PCPs in separation and catalysis.

Three-dimensional silica gel monoliths with a hierarchically macro-mesoporous structure are some of such porous materials and of high particular importance for real-world applications.[17,18] These monolithic silica materials are directly prepared through the alkoxysilane-derived sol–gel process accompanied by phase separation. In addition to the well-defined pore structure of the monoliths, their high enough mechanical strength is crucial to withstand the pressure of the fluids, which reaches 1 MPa at the linear velocity of 1 mm s⁻¹ in the case of 100 mm length monolithic silica columns.[19]

Recent developments in the synthesis strategy of the epoxide-mediated sol–gel accompanied by phase separation[20–24] have opened a pathway to transition metal hydroxide/oxyhydroxide monolithic gels, which otherwise end up with the crystalline precipitations. Syntheses of aluminum,[20] iron,[21] nickel,[22] chromium,[23] and copper[24] (oxy)hydroxide monoliths with well-defined macropores have been reported by this procedure.

In the case of PCPs, though monolithic materials with additional macropores would exhibit a high potential for enhancing their applicative domains, the direct synthesis has been still challenging because of the high tendency of PCP crystallites to precipitate as powders rather than to be integrated into a homogeneous monolithic form. Recently, the coordination replication technique, which allows the direct conversion of preformed three-dimensional macroporous metal oxide/hydroxide/oxyhydroxide monoliths into their corresponding PCP monoliths, was shown to be an alternative way to synthesize porous monolithic PCPs. Although promising, the scope of this technique has so far been limited to Al₂O₃ and V₂O₅.[25,26] The mechanical properties of the resultant PCP monoliths are, however, not satisfactory because of weak linkage between the PCP crystallites that constitute the macroporous framework. In the above cases of iron,[21] nickel,[22] chromium,[23] and copper[24] (oxy)hydroxide monoliths, polyacrylamide (PAAm), which is employed in the starting solution to induce phase separation, is found to take an additional part of "gluing" the (oxy)hydroxide colloidal constituents in the monolithic structure. The presence of PAAm in the original (oxy)hydroxide network may give a positive effect on the mechanical

[a] *Department of Chemistry, Graduate School of Science, Kyoto University, Kitashirakawa, Sakyo-ku, Kyoto 606-8502, Japan.*
E-mail: kanamori@kuchem.kyoto-u.ac.jp

[b] *Institute for Integrated Cell-Material Sciences (WPI-iCeMS), Kyoto University, Yoshida, Sakyo-ku, Kyoto 606-8501, Japan*

† Electronic supplementary information (ESI) available: Experimental details, an SEM image, and pore properties obtained from nitrogen adsorption–desorption. See DOI: 10.1039/c4cc09694k
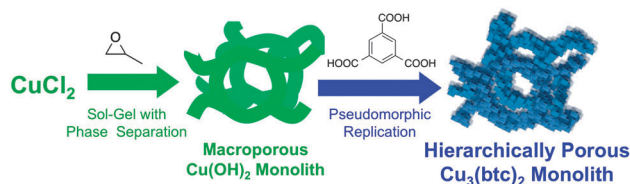
Fig. 1 Schematic representation of the synthesis of a $Cu(OH)_2$-based monolith and its coordination replication to a $Cu_3(btc)_2$ monolith in the presence of H_3btc with preserved macropores.

Fig. 2 Scanning electron micrographs of (a) Cu-03, (b) Cu-06, and (c) Cu-10, showing changes in the gel morphology and macropore size.

properties of final PCP monoliths, thus extending application forms of PCPs.

Using the copper hydroxide ($Cu(OH)_2$)-based monolith[24] as an example, we herein show the direct conversion into a corresponding PCP monolith by an acid–base reaction: $3Cu(OH)_2 + 2H_3btc \rightarrow Cu_3(btc)_2 + 6H_2O$ (btc = benzene-1,3,5-tricarboxylate), while preserving the well-defined co-continuous macroporous structure and monolithicity in the original gels (Fig. 1). The resultant $Cu_3(btc)_2$, also known as HKUST-1, is one of the most studied PCPs due to its high potential in catalysis and separation with coordinatively unsaturated sites.

As aforementioned, we have recently demonstrated a facile protocol for the synthesis of hierarchically porous copper hydroxide-based monoliths (amorphous), in which the microstructure and macropore size can be controlled.[24] Copper chloride and propylene oxide ($\pm$) were used as the metal source and acid scavenger, respectively.[27–29] The starting compositions for the synthesis of $Cu(OH)_2$-based monoliths are described in Table 1. The role of PAAm ($M_w = 10\,000$ Da) in the reaction mixture is not only controlling phase separation but also supporting the scaffold of $Cu(OH)_2$ by chelating the copper ions with nitrogen in the amide groups of PAAm, which is responsible for low crystallinity in the as-dried gels. Indeed, the precipitate was obtained when the reaction was conducted without the presence of PAAm (sample Cu-00). The addition of 0.30 g of PAAm (Cu-03, Fig. 2a) in the reaction mixture results in the formation of a monolithic gel. However, the gel morphology consists of aggregated particles due to high phase separation tendency. The increase in the amount of PAAm to 0.60 g (Cu-06, Fig. 2b) leads to the decreased phase separation tendency and a change in the gel morphology from aggregated particles to co-continuous structures with the macropore size of approximately 3 μm. The further increase in the amount of PAAm to 1.00 g (Cu-10, Fig. 2c) leads to a further decrease in phase separation tendency
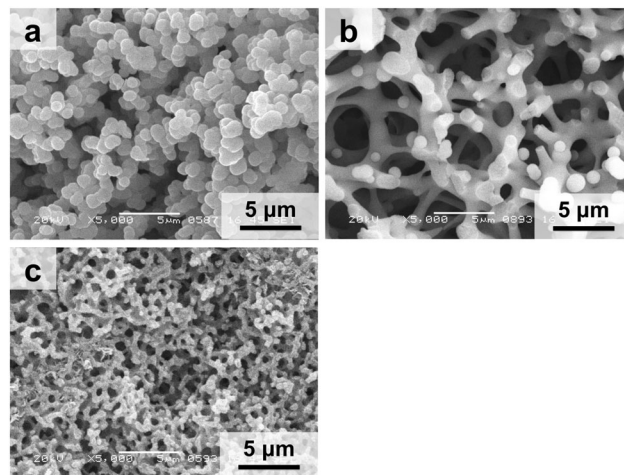
Table 1 Starting compositions and BET surface area (a_{BET}) values of the samples[a]

Entry	PAAm/g	$a_{BET}/m^2\ g^{-1}$	Morphology
Cu-00	0	N.A.	Precipitation
Cu-03	0.30	212	Particle aggregates
Cu-06	0.60	146	Co-continuous
Cu-10	1.00	97	Co-continuous

[a] In all the cases, 1.53 g of $CuCl_2 \cdot 2H_2O$, 1.10 mL of water, 0.30 mL of ethanol, 2.40 mL of glycerol and 1.47 mL of propylene oxide ($\pm$) were used for gel synthesis.

and the macropore size reduces to 0.5 μm. The nitrogen adsorption–desorption measurement of the as-synthesized gels reveals a decrease of the Brunauer–Emmett–Teller (BET) specific surface area with an increasing amount of PAAm in the gel network. The Barrett–Joyner–Halenda (BJH) pore size distribution curves derived from the adsorption branch reveal an increase in the most probable pore size with an increasing amount of PAAm from Cu-03 to Cu-10 (Fig. S1, ESI†).

The replication of the $Cu(OH)_2$ monolith to $Cu_3(btc)_2$ monolith was performed by immersing the as-synthesized Cu-06 in a solution containing 0.5 M H_3btc at 80 °C. We have screened out Cu-03 and Cu-10, since the precursor gel has low mechanical properties due to the low connectivity of macropore skeletons and too small macropores that easily collapse when the PCP crystallites develop with the reaction time, respectively. An immediate change in the color of the gel from green to blue with the preservation of the monolithic form indicates successful progression of conversion. The powder X-ray diffraction (XRD) of the dried gel unambiguously confirms the formation of $Cu_3(btc)_2$. In order to observe the course of conversion, we have optimized the reaction conditions by immersing 200 mg of as-dried Cu-06 in 5 mL of the 0.5 M H_3btc solution in N,N-dimethylformamide (DMF) and ethanol (1:1 by volume) at 80 °C. The progress of conversion with time was monitored by scanning electron microscopy (SEM, Fig. 3, and Fig. S2 in the ESI† at lower magnification), XRD (Fig. 4a), and nitrogen adsorption–desorption (Fig. 4b and c) of the samples at different time intervals.

The PCP daughter phase derived from the $Cu(OH)_2$-based monolith was observed by SEM after an immersion time of 2 min by roughening of the smooth parent surface, because of the surface-directed growth of small ill-defined nuclei of sub-100 nm. The XRD of the gel after 2 min also indicated the change from amorphous to slightly crystalline in the gel; these observations are supported by an increase in the surface area contributed mostly by the increased microporosity of $Cu_3(btc)_2$. Upon increasing the reaction time to 3 and 6 min, the population of well-defined sub-micrometer-sized PCP crystals and the microporosity were further increased with the preservation of
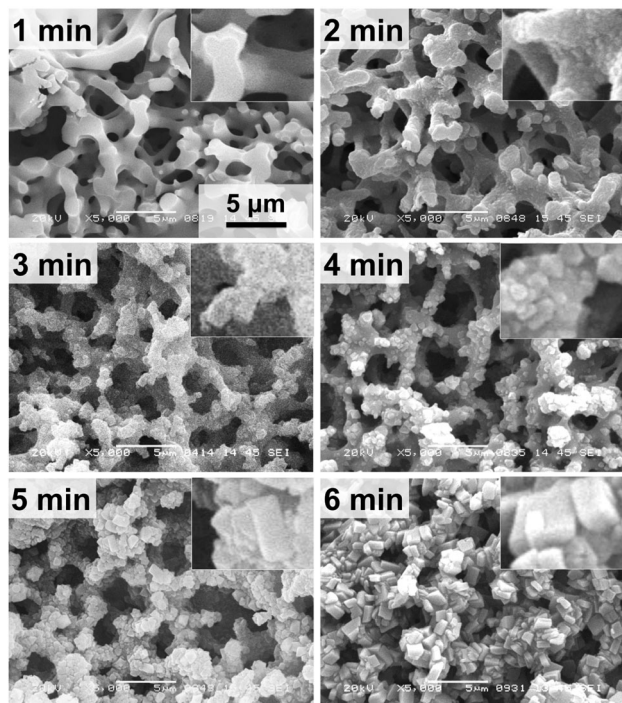
Fig. 3 SEM images of the conversion of Cu-06 to $Cu_3(btc)_2$ with 1 minute time intervals, showing the growth of polyhedral crystallites with the preservation of the co-continuous macroporous gel structure. All the images are in the identical magnification.
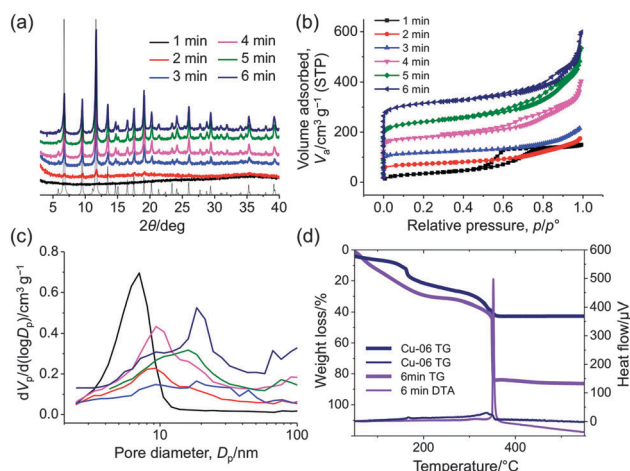

Fig. 4 (a) XRD patterns (Cu Kα) of Cu-06 in the course of coordination replication recorded at 1 minute time intervals. A simulated pattern is also shown at the bottom; (b) nitrogen adsorption–desorption isotherms of the same samples; (c) BJH pore size distribution of the samples; (d) TG-DTA results of the samples before (Cu-06) and after conversion (6 min), showing an increase in the organic content.

the parent co-continuous macroporous structure. After a reaction time of 6 min, densely packed crystals with the parent macroporous architecture were obtained. This is also supported by the XRD results, which demonstrate the appearance of a highly crystalline $Cu_3(btc)_2$ phase. The highly crystalline and porous daughter phase causes a decrease in the macropore size. The progress of the reaction stopped at this stage and the total specific surface area reaches
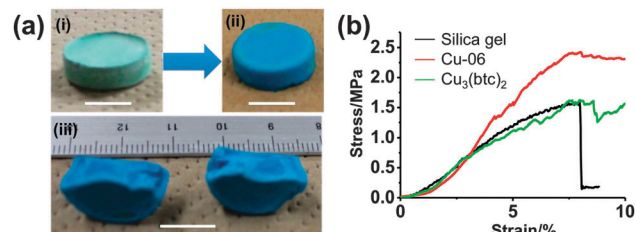

Fig. 5 (a) Photographs of as-dried Cu-06 monolith (i) before and (ii) after conversion to the $Cu_3(btc)_2$ monolith, (iii) cross-section of the $Cu_3(btc)_2$ monolith shows uniform replication throughout the monolith (the scale bars correspond to 1 cm); (b) stress–strain curves of Cu-06, after conversion to $Cu_3(btc)_2$ (6 min), and a macroporous silica monolith with SBA-15-like periodic mesopores.

1315 $m^2 g^{-1}$ (Table S1, ESI†), which is comparable to the $Cu(OH)_2$-derived $Cu_3(btc)_2$ powders[30] and remains almost constant even after a reaction time of 24 h, indicating the total possible conversion of $Cu(OH)_2$ monoliths. The extension of the mesopore size is attributed to the interstitial pores formed in-between the $Cu_3(btc)_2$ crystallites in the macropore skeletons. An increase in the incorporation of H_3btc in the gel network was confirmed by thermogravimetry-differential thermal analysis (TG-DTA), which shows a sharp weight loss at around 375 °C (Fig. 4d). In all the cases, crack-free monoliths were obtained after solvent exchange with ethanol and drying at 40 °C for 1 d. It is noteworthy that the kinetics of coordination replication depends also on the dimension of the monolith. The increase in the replication time with increasing dimension of the monolith is attributed to the extended time required for diffusion of the ligand inside the monolith. It took 30 min for complete replication when using a cylinder-shaped monolith with a diameter of 1 cm and a height of 0.5 cm (Fig. 5a).

The monoliths were then subjected to mechanical measurement by uniaxial compression. For this study, a macroporous silica monolith with SBA-15-type periodic mesoporosity,[31] which has been used as a stationary phase for high-performance liquid chromatography (HPLC),[32] has been used as a reference to compare the mechanical properties of as-dried Cu-06 and the $Cu_3(btc)_2$ monolith (reacted for 6 min). Although a decrease in strength (stress values at catastrophic failure) is found from ~2.5 MPa for $Cu(OH)_2$ to ~1.5 MPa for $Cu_3(btc)_2$ as shown in Fig. 5b, the value is still well comparable to that of the periodic mesoporous silica monolith (strength ~1.5 MPa). This result promises the uses under liquid flow by pumping such as chromatography columns and continuous flow reactors.[33,34] The decrease in Young's modulus and compressive strength is probably due to the lowered connectivity between the $Cu_3(btc)_2$ crystallites formed by the transformation; however, the presence of a small amount of PAAm in the skeletons should enhance the binding of each crystallite to increase the toughness of the monolith just as in the case of $Cu_3(btc)_2$-based hollow capsules supported by 4 wt% of polyvinyl alcohol.[5] Although other reported MOF–polymer composites[35–37] may show higher mechanical stability because they consist mostly of the polymer, their accessible surface area is limited to around 500 $m^2 g^{-1}$ or less, which is lower than 1315 $m^2 g^{-1}$ in our case.

In summary, we have demonstrated the direct conversion of hierarchically porous $Cu(OH)_2$-based monoliths to $Cu_3(btc)_2$

(HKUST-1) monoliths by coordination replication in the presence of H$_3$btc as the ligand with complete preservation of the macroporous structure. After 6 min of the conversion treatment, the resulting Cu$_3$(btc)$_2$ monolith shows high crystallinity, a high surface area of 1315 m^2 g^{-1}, and high enough mechanical properties. These properties make this material attractive for future applications as the heterogeneous monolithic catalyst that can be used in the continuous flow mode.

Notes and references

1 S. Kitagawa, R. Kitaura and S. Noro, *Angew. Chem., Int. Ed.*, 2004, **43**, 2334–2375.
2 G. Ferey, *Chem. Soc. Rev.*, 2008, **37**, 191–214.
3 J. R. Long and O. M. Yaghi, *Chem. Soc. Rev.*, 2009, **38**, 1213–1214.
4 A. Carne-Sanchez, I. Imaz, M. Cano-Sarabia and D. Maspoch, *Nat. Chem.*, 2013, **5**, 203–211.
5 R. Ameloot, F. Vermoortele, W. Vanhove, M. B. J. Roeffaers, B. F. Sels and D. E. De Vos, *Nat. Chem.*, 2011, **3**, 382–387.
6 L. He, Y. Liu, J. Liu, Y. Xiong, J. Zheng, Y. Liu and Z. Tang, *Angew. Chem., Int. Ed.*, 2013, **52**, 3741–3745.
7 R. Makiura, S. Motoyama, Y. Umemura, H. Yamanaka, O. Sakata and H. Kitagawa, *Nat. Mater.*, 2010, **9**, 565–571.
8 O. Shekhah, J. Liu, R. A. Fischer and C. Woell, *Chem. Soc. Rev.*, 2011, **40**, 1081–1106.
9 A. M. Doherty, G. Grenci, R. Ricco, J. I. Mardel, J. Reboul, S. Furukawa, S. Kitagawa, A. J. Hill and P. Falcaro, *Adv. Mater.*, 2013, **25**, 4701–4705.
10 P. Küsgens, A. Zgaverdea, H.-G. Fritz, S. Siegle and S. Kaskelw, *J. Am. Ceram. Soc.*, 2010, **93**, 2476–2479.
11 L. Li, S. L. Xiang, S. Q. Cao, J. Y. Zhang, G. F. Ouyang, L. P. Chen and C. Y. Su, *Nat. Commun.*, 2013, **4**, 1774.
12 D. Zacher, O. Shekhah, C. Woell and R. A. Fischer, *Chem. Soc. Rev.*, 2009, **38**, 1418–1429.
13 M. E. Silvestre, M. Franzreb, P. G. Weidler, O. Shekhah and C. Woll, *Adv. Funct. Mater.*, 2013, **23**, 1210–1213.
14 Y. Hu, X. Dong, J. Nan, W. Jin, X. Ren, N. Xu and Y. M. Lee, *Chem. Commun.*, 2011, **47**, 737–739.
15 D. Witters, N. Vergauwe, R. Ameloot, S. Vermeir, D. De Vos, R. Puers, B. Sels and J. Lammertyn, *Adv. Mater.*, 2012, **24**, 1316–1320.
16 S. Furukawa, J. Reboul, S. Diring, K. Sumida and S. Kitagawa, *Chem. Soc. Rev.*, 2014, **43**, 5700–5734.
17 K. Nakanishi, *J. Porous Mater.*, 1997, **4**, 67–112.
18 K. Nakanishi and N. Tanaka, *Acc. Chem. Res.*, 2007, **40**, 863–873.
19 H. Minakuchi, K. Nakanishi, N. Soga, N. Ishizuka and N. Tanaka, *Anal. Chem.*, 1996, **68**, 3498–3501.
20 Y. Tokudome, K. Fujita, K. Nakanishi, K. Miura and K. Hirao, *Chem. Mater.*, 2007, **19**, 3393–3398.
21 Y. Kido, K. Nakanishi, A. Miyasaka and K. Kanamori, *Chem. Mater.*, 2012, **24**, 2071–2077.
22 Y. Kido, K. Nakanishi, N. Okumura and K. Kanamori, *Microporous Mesoporous Mater.*, 2013, **176**, 64–70.
23 Y. Kido, G. Hasegawa, K. Kanamori and K. Nakanishi, *J. Mater. Chem. A*, 2014, **2**, 745–752.
24 S. Fukumoto, K. Nakanishi and K. Kanamori, under review.
25 J. Reboul, S. Furukawa, N. Horike, M. Tsotsalas, K. Hirai, H. Uehara, M. Kondo, N. Louvain, O. Sakata and S. Kitagawa, *Nat. Mater.*, 2012, **11**, 717–723.
26 J. Reboul, K. Yoshida, S. Furukawa and S. Kitagawa, *CrystEngComm*, 2015, **17**, 323–330.
27 H. Itoh, T. Tabata, M. Kokitsu, N. Okazaki, Y. Imizu and A. Tada, *J. Ceram. Soc. Jpn.*, 1993, **101**, 1081–1083.
28 A. E. Gash, T. M. Tillotson, J. H. Satcher, Jr., J. F. Poco, W. L. Hrubesh and R. L. Simpson, *Chem. Mater.*, 2001, **13**, 999–1007.
29 A. E. Gash, T. M. Tillotson, J. H. Satcher Jr., L. W. Hrubesh and R. L. Simpson, *J. Non-Cryst. Solids*, 2001, **285**, 22–28.
30 G. Majano and J. Perez-Ramirez, *Adv. Mater.*, 2013, **25**, 1052–1057.
31 T. Amatani, K. Nakanishi, K. Hirao and T. Kodaira, *Chem. Mater.*, 2005, **17**, 2114–2119.
32 Y. Zhu, K. Morisato, K. Kanamori and K. Nakanishi, *ACS Appl. Mater. Interfaces*, 2013, **5**, 2118–2125.
33 A. Sachse, R. Ameloot, B. Coq, F. Fajula, B. Coasne, D. De Vos and A. Galarneau, *Chem. Commun.*, 2012, **48**, 4749–4751.
34 N. Moitra, K. Kanamori, Y. H. Ikuhara, X. Gao, Y. Zhu, G. Hasegawa, K. Takeda, T. Shimada and K. Nakanishi, *J. Mater. Chem. A*, 2014, **2**, 12535–13544.
35 L. D. O'Neill, H. Zhang and D. Bradshaw, *J. Mater. Chem.*, 2010, **20**, 5720–5726.
36 R. Ostermann, J. Cravillon, C. Weidmann, M. Wiebcke and B. M. Smarsly, *Chem. Commun.*, 2011, **47**, 442–444.
37 M. L. Pinto, S. Dias and J. Pires, *ACS Appl. Mater. Interfaces*, 2013, **5**, 2360–2363.